# Wireless Power Transfer via Magnetic Resonance Coupling (MRC) with Reduced Standby Power Consumption

Byoung-Hee Lee[†]

[†]Department of Electronics and Control Engineering, Hanbat National University, Daejeon, Korea

## Abstract

Wireless power transfer (WPT) technology with various transfer mechanisms such as inductive coupling, magnetic resonance and capacitive coupling is being widely researched. Until now, power transfer efficiency (PTE) and power transfer capability (PTC) have been the primary concerns for designing and developing WPT systems. Therefore, a lot of studies have been documented to improve PTE and PTC. However, power consumption in the standby mode, also defined as the no-load mode, has been rarely studied. Recently, since the number of WPT products has been gradually increasing, it is necessary to develop techniques for reducing the standby power consumption of WPT systems. This paper investigates the standby power consumption of commercial WPT products. Moreover, a standby power reduction technique for WPT systems via magnetic resonance coupling (MRC) with a parallel resonance type resonator is proposed. To achieve a further standby power reduction, the voltage control of an AC/DC travel adapter is also adopted. The operational principles and characteristics are described and verified with simulation and experimental results. The proposed method greatly reduces the standby power consumption of a WPT system via MRC from 2.03 W to 0.19 W.

**Key words:** Class-E power amplifier, Magnetic resonance coupling (MRC), Parallel resonance type resonator, Standby power, Travel adapter, Wireless power transfer (WPT)

## I. INTRODUCTION

Recently, rechargeable batteries have become a major power source for various electronics devices from low power systems such as smartphones, laptop computers and wearable devices to high power systems such as electric vehicles (EVs). There are two possible charging mechanisms, wired charging and wireless charging. Wireless charging is increasingly applied to various applications due to its usefulness and convenience. Wireless charging can be implemented with different wireless power transfer (WPT) technologies, i.e., inductive coupling, magnetic resonance and capacitive coupling [1].

The operational modes of a WPT system can be divided into a power transfer mode called the normal mode and a standby mode called the no-load mode. In the power transfer mode, a relatively large power for supplying load power is transferred from a transmitter (Tx) to a receiver (Rx). Thus, power transfer efficiency (PTE) is an important issue in the power transfer mode. Moreover, robustness of operation with large spatial misalignments and load variations is required [10]-[12]. In the standby mode, Tx continually consumes an amount of power to detect the existence of a proper Rx, which is located within an available charging range of Tx. Since there is no power transfer from Tx to Rx, the consumed power of Tx during the standby mode, defined as the standby power or no-load power, is considered to be a waste of energy. When the number of WPT systems increases, the standby power of the WPT systems is also expected to increase [1]. However, most of the previous studies were focused on improving the PTE or PTC such as robustness with spatial misalignment. Therefore, it is attractive to develop a standby power reduction technique for WPT systems. This paper is an extended version of a conference paper that was presented at the IEEE WPTC (Wireless Power Transfer Conference) 2016 [13]. In this paper,

the standby power consumption of commercial WPT products is investigated. The proposed standby power reduction method for WPT systems, which is based on an analysis of impedance behavior depending on the type of resonator, is described. The operational principles and characteristics of the proposed technique are described in detail. Moreover, an additional standby power reduction technique is adopted to achieve a further reduction of the standby power. The proposed method is verified by computer-based simulation (PSIM) and experimental results. When compared with the previously reported results in the conference paper, the final proposed WPT system further reduces the total standby power consumption.

## II. STANDBY POWER CONSUMPTION OF COMMERCIAL WPT PRODUCTS

Until now, all of the commercially available WPT products have been based on a WPT technique via inductive coupling that has been standardized by the wireless power consortium (WPC), called Qi [14]. To understand the current status of the standby power consumption of commercial products, standby power consumption has been measured. The measured power consumption of all products is from 0.13 W to 0.25 W.

Although the WPT technique via inductive coupling has a high PTE and has been commercialized, the small spatial freedom of the power transfer limits the application of this technology. To overcome this limitation, WPT techniques via MRC and other techniques such as via radio-frequency, optical or ultrasound have been studies. Among them, WPT via MRC has drawn a great deal of attention due to its larger spatial freedom. This WPT technique has been standardized by Airfuel [15]. Thus, in the following sections, the proposed standby power techniques are targeted to the WPT technique via MRC.

## III. ANALYSIS OF IMPEDANCE BEHAVIORS WITH VARIOUS TYPES OF RESONATORS

Fig. 1 shows a conventional structure of a WPT system via MRC and it is composed of a DC-AC inverter for generating an alternating current (AC) from a direct current (DC) source $V_S$, which is generally supplied from an AC/DC travel adapter. Fig. 2 shows a class-E power amplifier with a 2nd harmonic filter. This is widely adopted for DC-AC inverters due to its simple structure and high efficiency [16]-[24]. A 2nd harmonic filter, which is made up of $L_2$ and $C_2$, is generally adopted to reduce the highest harmonics. An Rx resonator receives power that was transmitted from Tx. A rectifier rectifies the received AC power by the Rx resonator to the DC voltage. A DC-DC converter regulates the output voltage required by a load system. The DC/DC converter can be implemented with a non-isolated type DC-DC converter such as a buck, boost or
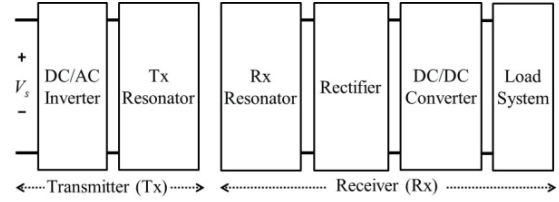


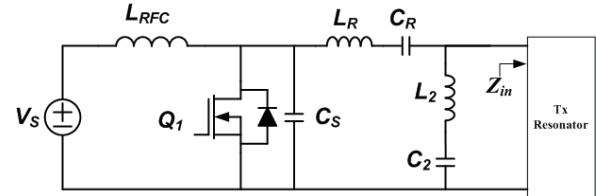Fig. 1. Conventional structure of a WPT system via MRC.



Fig. 2. Circuit diagram of an class-E power amplifier with a 2nd harmonic filter.

buck-boost converter. A buck DC-DC converter is adopted since the output voltage of the rectifier is higher than the required voltage of the load system. The selection of the DC-DC converter depends on the requirements of the load system [25], [26].

For simplification of analysis, the rectifier, the DC-DC converter and the load system are usually modeled as an equivalent load resistance, $R_{load}$ [17]. Since resonators can be implemented with a combination of series and parallel types, four types of Tx-Rx resonators can be implemented. Fig. 3 shows a basic resonator with $R_{load}$, and a mutual inductance $M$ that is expressed as follows:

$$M = k\sqrt{L_{Tx}L_{Rx}} \tag{1}$$

where $k$ is a coupling coefficient between the Tx resonator and the Rx resonator, $L_{Tx}$ is the self-inductance of the Tx resonator and $L_{Rx}$ is the self-inductance of the Rx resonator.

Fig. 4(a) and Fig. 4(b) show the loaded equivalent circuit with a reflected impedance $Z_r$ for the series and parallel types of Tx, respectively. $Z_r$ is determined by $k$ and the operating angular frequency $\omega$ as expressed in Equ. (2):

$$Z_r = \omega^2 M^2 / Z_{Rx} \tag{2}$$

where $Z_{Rx}$ is the total impedance of the Rx resonator and $R_{load}$.

With $Z_r$, the total equivalent input impedance at the Tx resonator $Z_{in}$ can be expressed as follows:

$$Z_{in} = \begin{cases} \frac{1}{j\omega C_{Tx}} + j\omega L_{Tx} + Z_r & : \text{series type of Tx} \\ \frac{1}{j\omega C_{Tx} + \frac{1}{j\omega L_{Tx} + Z_r}} & : \text{parallel type of Tx} \end{cases} \tag{3}$$

where $C_{Tx}$ is the capacitance of the Tx resonator.

Fig. 5 shows the correlation of the impedance and output power of a class-E power amplifier with a 2nd harmonic filter under a fixed operating frequency and input voltage. The real part of $Z_{in}$ represents the real power of the class-E power amplifier, while the imaginary part of $Z_{in}$ indicates the reactive
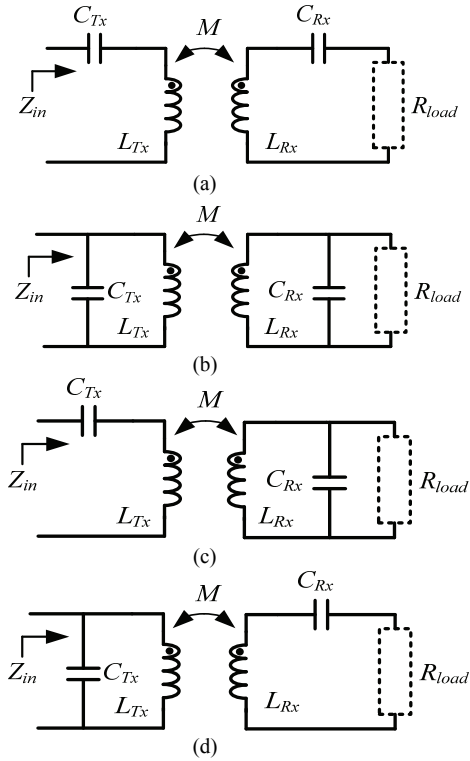
(a)

(b)

(c)

(d)

Fig. 3. Four types of Tx-Rx resonators. (a) Series-series. (b) Parallel-parallel. (c) Series-parallel. (d) Parallel-series.
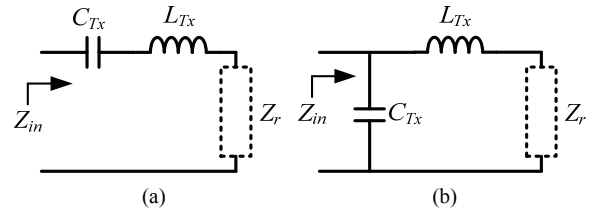


(a)       (b)

Fig. 4. Loaded equivalent circuit according to the Tx resonator type. (a) Series type of Tx. (b) Parallel type of Tx.
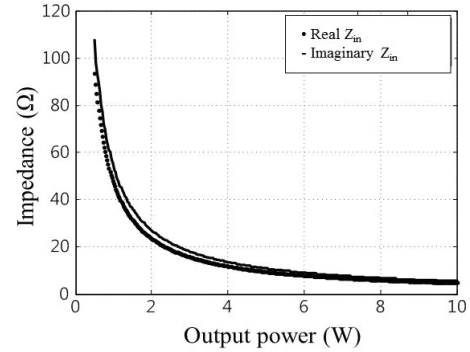


Fig. 5. Correlation between impedance and output power.

TABLE I
SUMMARY OF POWER CORRELATION

| Type of Resonator | Power Correlation | | | | | |
| --- | --- | --- | --- | --- | --- | --- |
| | $R_{load}$ | $k$ | Required real power, $P_1$ | Real $Z_{in}$ | Real power of power amplifier, $P_2$ | Coincidence, $P_1$ and $P_2$ |
| series-series | ↑ | constant | ↓ | ↓ | ↓ | O |
| | constant | ↓ | ↑ | ↓ | ↓ | X |
| series-parallel | ↑ | constant | ↓ | ↑ | ↑ | X |
| | constant | ↓ | ↑ | ↓ | ↓ | X |
| parallel-series | ↑ | constant | ↓ | ↓ | ↓ | O |
| | constant | ↓ | ↑ | ↑ | ↓ | X |
| parallel-parallel | ↑ | constant | ↓ | ↓ | ↓ | O |
| | constant | ↓ | ↑ | ↑ | ↑ | O |

power. In order to maximize the efficiency of the class-E power amplifier [16], the operating frequency is designed at the resonance frequency $\omega_0$, which is given by:

$$\omega_0 = 1\Big/\sqrt{L_{Tx}C_{Tx}} = 1\Big/\sqrt{L_{Rx}C_{Rx}} \qquad (4)$$

where $C_{Rx}$ is the capacitance of the Rx resonator.

When the real part of $Z_{in}$ increases, the output power of a class-E power amplifier decreases as shown in Fig. 5. Since the real part of $Z_{in}$ is determined by Equ. (2) and Equ. (3), $Z_{in}$ is affected by $k$, $R_{load}$ and type of resonator. Table I shows a summary of the power correlation between the required real power of Tx, $P_1$, and the real power of a class-E power amplifier with variation of the system parameters, $P_2$. The

upward arrow and the downward arrow refer to an increase of value and a decrease of value, respectively. Moreover, 'O' is the coincidence between $P_1$ and $P_2$. 'X' is the discordance of the values. The series-series type resonator is incompatible with variations of the coupling coefficient. Thus, to compensate for the difference between the required load power and the reduced transmitted power, an additional DC-DC converter is usually applied to control the input voltage $V_S$ [20]. However, this degrades the system efficiency and compactness. On the other hand, the parallel-parallel type resonator has proper power correlation characteristics with variations of $k$ and $R_{load}$ as shown in Table I. Thus, to develop a compact and cost-effective WPT system, a parallel-parallel resonator is the proper type of resonator among the four types of basic resonators. However,

since the real part of $Z_{in}$ greatly increases as described in Equ. (2) and Equ. (3) in the standby mode, the transmitted output power of a WPT system with the parallel-parallel type of resonator increases extremely. Therefore, the standby power reduction of a WPT system with the parallel-parallel type of resonator is required. To reduce the power consumption of a WPT system with the parallel-parallel type of resonator in the standby mode, standby power reduction techniques are proposed and explained in the following section.

## IV. PROPOSED STANDBY POWER REDUCTION TECHNIQUES

### A. Standby Power Reduction with an Impedance Inversion Circuit

A WPT system with a parallel-parallel resonator has a large standby power consumption due to the power correlation characteristics as described in section III. Fig. 6 shows the proposed WPT system structure for reducing standby power consumption. The proposed technique takes advantage of an impedance inversion circuit that is made up of an inductor $L_3$, a capacitor $C_3$ and a control switch $Q_3$. With the impedance inversion circuit shown in Fig. 6, the equivalent load impedance $Z_{in\_eq}$ can be expressed as follows:

$$Z_{in\_eq} = \frac{(1-\omega^2 L_3 C_3 Z_{in})(1-\omega^2 L_3 C_3)-j\omega Z_{in}C_3}{(1-\omega^2 L_3 C_3)^2+(\omega Z_{in}C_3)^2}. \quad (5)$$

Due to the square term of $Z_{in}$ in the denominator, as described in Equ. (5), the impedance inversion circuit inverts the change tendency of $Z_{in\_eq}$ when compared to that of $Z_{in}$. Moreover, it can filter out the 3rd harmonics generated by the transmitter in the standby mode. The impedance inversion circuit can be implemented with other structures such as a simple capacitor $C_3$ and a switch $Q_3$ as shown in Fig. 7. With the simple impedance inversion circuit, $Z_{in\_eq}$ can be expressed as follows:

$$Z_{in\_eq} = \frac{Z_{in}-j\omega Z_{in}^2 C_3}{1+(\omega Z_{in}C_3)^2}. \quad (6)$$

As described in Equ. (6), the simple impedance inversion circuit can also invert the change tendency of $Z_{in\_eq}$, due to the square term of $Z_{in}$ in the denominator. In this paper, to further mitigate the harmonic issue of a WPT system, the 3rd harmonic filter type of impedance inversion circuit is employed as shown in Fig. 6. Since the impedance inversion circuit reverses the change tendency of $Z_{in\_eq}$ when compared to that of $Z_{in}$ under variations of the system parameters, the proposed WPT system structure can reduce power consumption in the standby mode.

To implement the impedance inversion circuit, the on/off control of $Q_3$ is required. In a WPT system via MRC, BLE (Bluetooth low energy) is adopted for wireless data communication and the main controller. $Q_3$ is turned-on or turned-off by control signals from the BLE at Tx. Under normal conditions, since power is transferred from Tx to Rx,
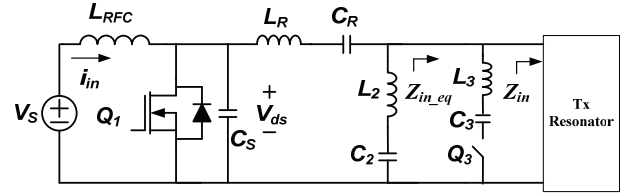


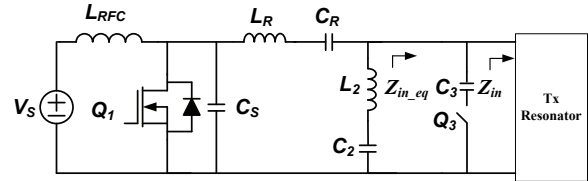Fig. 6. Proposed WPT system structure for reducing standby power consumption.



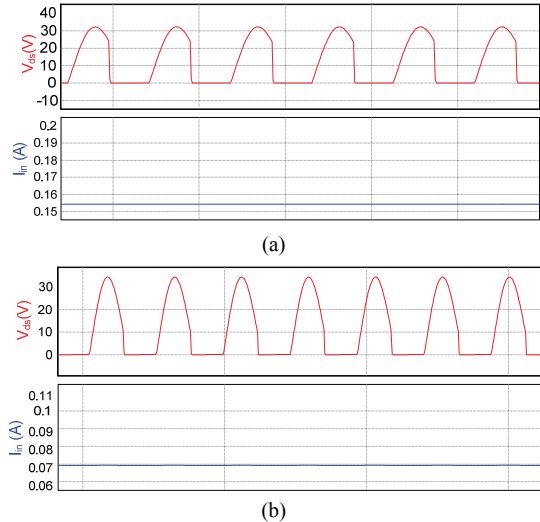Fig. 7. Structure of a WPT system with a simple impedance inversion circuit.



Fig. 8. Simulation results. (a) Conventional WPT system. (b) Proposed WPT system.

Tx and Rx can communicate appropriately by the BLE. In this case, the BLE at Tx generates the turn-off signals for $Q_3$. Under the no-load or standby condition, since there is only Tx, communication by the BLE is disconnected. Thus, the BLE at Tx generates the turn-on signals for $Q_3$.

Based on a PSIM simulation, a conventional WPT system has 1.8 W standby power consumption. By adopting the proposed circuit shown in Fig. 6, the standby power consumption is reduced to 0.83 W. Fig. 8 shows simulation results with the system specifications in Table II and the system parameters in Table III. The standby power consumption can be also reduced by adopting a simple impedance inversion circuit. However, the standby power of the proposed system is larger than the 0.45 W of standby power required in the latest Energy Star Program [27]. Moreover, since minimizing the standby power consumption
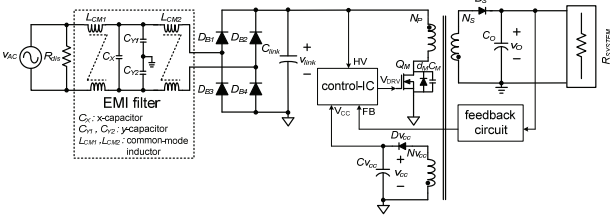
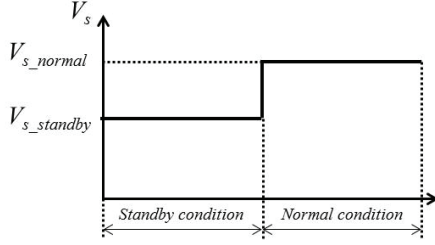Fig. 9. Structure of a conventional AC/DC travel adapter [28].



Fig. 10. Operational principle of the output voltage control method.
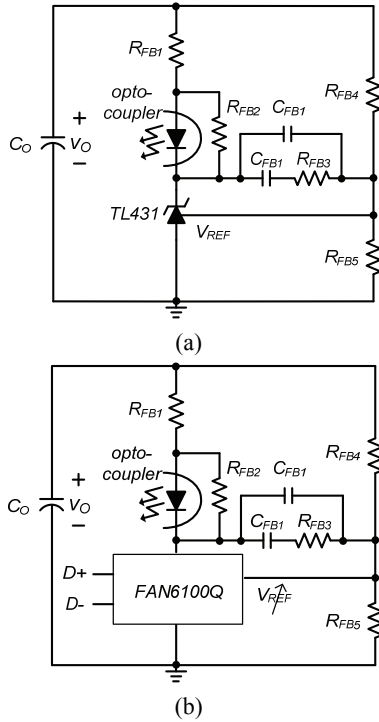


(a)



(b)

Fig. 11. Implementation example of feedback circuits. (a) Conventional feedback circuit. (b) Feedback circuit for output voltage control.

of power systems is continuously required, an additional method is proposed for a further reduction of standby power in the following section.

### B. Additional Standby Power Reduction Method with the Voltage Control of an AC/DC Adapter

The output power of a class-E power amplifier is a function of the input voltage $V_S$ and the parallel capacitance $C_S$ [16]. In a conventional WPT system, $V_S$ is supplied from an AC/DC travel adapter as described in section III. Generally, the AC/DC travel adapter supplies a constant output voltage and a variable output current according to the required load power. Fig. 9 shows a circuit diagram of a conventional AC/DC travel adapter [28]. It converts universal AC voltages such as 90 $V_{AC,RMS}$ ~ 264 $V_{AC,RMS}$ to a required DC voltage such as 12 V. Since the output voltage of a AC/DC travel adapter $v_O$ is maintained at constant voltage regardless of the load condition, it can increase the power consumption of a class-E power amplifier at the standby condition. To further reduce standby power consumption, the output voltage control method of an AC/DC travel adapter is adopted in the proposed WPT system. The operational principle of the output voltage control method is briefly described in Fig. 10. Under normal conditions, $v_O$ is sustained at its normal output voltage $V_{s\_normal}$ to supply sufficient load power. During the standby mode, $v_O$ decreases to a certain level $V_{s\_standby}$, which can guarantee the primary operation of the WPT system. By decreasing the $v_O$ of the AC/DC travel adapter, since the power consumption of a class-E power amplifier is proportional to the input voltage of a class-E power amplifier [16], it can be reduced. In this paper, since the minimum operating voltage of the control circuit is 5 V, $V_{s\_standby}$ is selected as 5 V. To control the $v_O$ of the AC/DC travel adapter, the feedback circuit of the AC/DC travel adapter is revised as shown in Fig. 11. Fig. 11 (a) shows the conventional feedback circuit of an AC/DC travel adapter. $v_O$ can be expressed as follows:

$$v_o = \left(1 + \frac{R_{FB5}}{R_{FB4}}\right) V_{REF}. \tag{7}$$

Since $R_{FB4}$, $R_{FB5}$ and $V_{REF}$ are fixed values in the conventional AC/DC travel adapter, $v_O$ is regulated at a constant value [29]. To control $v_O$, it is necessary to change the value of one of them. Since FAN6100Q can manage $V_{REF}$ from 1 V to 2.4 V according to the communication signal by D+ and D- [30], a method for controlling $V_{REF}$ is adopted in the proposed system as shown in Fig. 11 (b). In the normal mode, since $V_{REF}$ is retained at 2.4 V, $v_O$ is regulated at 12 V with the feedback resistors described in Table III. In the standby mode, when $V_{REF}$ is lowered to 1 V, $v_O$ is regulated at 5 V.

## V. EXPERIMENTAL RESULTS

To verify the proposed standby power reduction technique, a 10 W experimental prototype of a WPT system is implemented. The system specifications are presented in Table II. With a modification of the design procedures presented in [16]-[24], the experimental circuit parameters are listed in Table III. The switching frequency is determined as 6.78 MHz according to the specifications of AirFuel [15].

Fig. 12 shows a photograph of the experimental set-up of the proposed method with a 3rd harmonic filter type of

TABLE II
SYSTEM SPECIFICATIONS

| Parameters | Value |
|---|---|
| Input voltage at Normal condition, $V_{s\_normal}$ | 12 V |
| Input voltage at standby condition, $V_{s\_standby}$ | 5 V |
| Rated Output Power, $Po$ | 10 W |
| Switching frequency, $Fs$ | 6.78 MHz |

TABLE III
CIRCUIT PARAMETERS

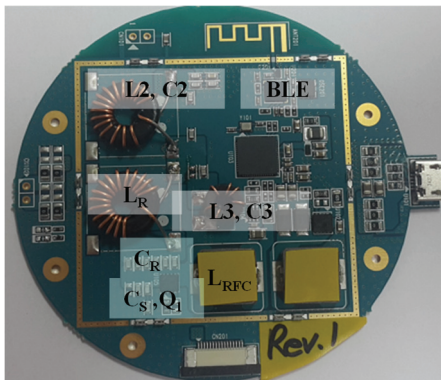| Parameters | Value |
|---|---|
| Radio frequency choke, $L_{RFC}$ | 6.8 uH |
| Main power switch, $Q_1$ | FDMC8622 |
| Additional parallel capacitor, $C_S$ | 520 pF |
| Additional resonance filter, $L_R$ & $C_R$ | 1800 nH / 450 pF |
| 2nd harmonic resonance filter, $L_2$ & $C_2$ | 175 nH / 790 pF |
| Impedance inversion circuit, $L_3$ & $C_3$ | 70 nH / 920 pF |
| Output voltage control IC of AC/DC travel adapter | FAN6100Q |
| Feedback resistor, $R_{FB4}$ & $R_{FB5}$ | 30 kΩ & 7.5 kΩ |



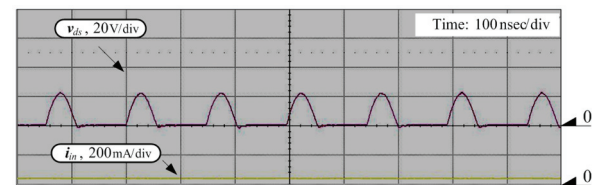Fig. 12. Experimental set-up of the proposed method.
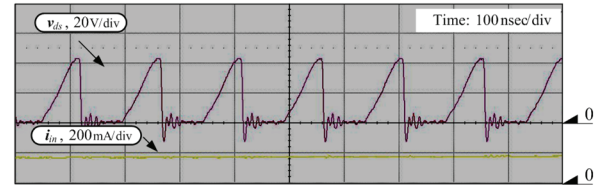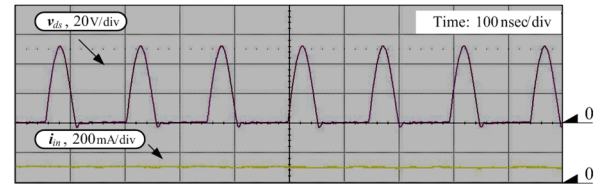


Fig. 13. Experimental waveforms of the switch voltage ($v_{ds}$) and input current ($i_{in}$). (a) Conventional system. (b) Proposed system with an impedance inversion circuit.
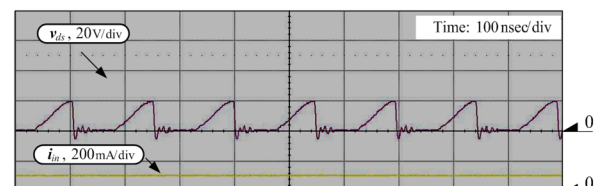


Fig. 14. Experimental waveforms of the switch voltage ($v_{ds}$) and input current ($i_{in}$). (a) Conventional system with the additional standby power reduction method. (b) Proposed system with an impedance inversion circuit and the additional standby power reduction method.

TABLE IV
CALCULATED POWER LOSS DISTRIBUTION

| Parameters | Conventional | Proposed | Formula |
|---|---|---|---|
| Choke inductor, $L_{RFC}$ | 2.2 mW | 0.1 mW | $P_{loss\_1} = I_{rms}^2 \times R_{on}$ |
| Power switch, $Q_1$ | 823 mW | 67.9 mW | $P_{loss\_2} = I_{rms}^2 \times R_{on} + Q_{gate} \times V_{gate} \times F_s + C_{OSS} \times V_{ds}^2 \times F_s$ |
| Resonance filter, $L_R$ & $C_R$ | 7 mW | 5 mW | $P_{loss\_3} = I_{rms}^2 \times R_{on}$ |
| Estimated power loss, $P_{LOSS}$ | 832.2 mW | 73 mW | $\sum_{x=1}^{3} P_{loss\_x}$ |

impedance inversion circuit. Experimental waveforms of the switch voltage and input current of the implemented WPT system are shown in Fig. 13. The measured standby power consumption of the WPT system without the proposed method is 2.03 W. With the proposed impedance inversion circuit, the standby power consumption decreases from 2.03 W to 1.17 W as described in section IV. These experimental results are slightly larger than the obtained simulation results due to the power loss of the auxiliary circuits for communication and protection. Moreover, with the additional standby power reduction method, the final standby power consumption is 0.19 W as shown in Fig. 14. The calculated power loss distributions are compared in Table IV. By adapting the proposed technique, the loss of $Q_1$ is greatly

reduced due to the soft-switching characteristic as shown in Fig. 14. Although the total standby power consumption is a little bit larger than that of the conventional WPT system via inductive coupling described in Section II, the proposed technique satisfies the standby power requirements of the latest Energy Star Program [27].

## VI. CONCLUSIONS

In this paper, a standby power reduction technique for WPT systems is proposed. Based on an analysis of the impedance characteristics according to variations of the system parameters, a parallel resonance type resonator is adopted to develop a compact and high efficiency WPT system. The proposed technique can reduce the standby power consumption of the WPT system by adopting an impedance inversion circuit. Moreover, to achieve a further reduction of standby power, the voltage control method of an AC/DC travel adapter is also adopted. The operational principle and characteristics of the proposed techniques are described in detail. The proposed techniques are verified by simulation and experimental results. Therefore, it is expected that the proposed techniques can reduce standby power for various WPT systems via MRC.

## ACKNOWLEDGMENT

## REFERENCES

[1]  Markets and Markets, *Wireless Power Transmission Market by Technology (Induction & Magnetic, Resonance), Implementation, Receiver & Transmitter Application (Smartphones, Wearable Electronics, Electric Vehicles & Furniture), and Region – Global Trend and Forecast to 2020*, Jan. 2016.

[2]  N. Tesla, The Transmission of Electric Energy without Wire*s*, *The Electrical World and Engineer*. New York, NY, USA: McGraw-Hill, Mar. 5, 1904.

[3]  A. Kurs, A. Karalis, R. Moffatt, J. D. Joannopoulos, P. Fisher, and M. Soljacic, "Wireless power transfer via strongly coupled magnetic resonances," *Science*, Vol. 317, No. 5834, pp. 83-86, Jun. 2007.

[4]  S. Y. R. Hui, W. Zhong, and C. K. Lee, "A critical review of recent progress in mid-range wireless power transfer," *IEEE Trans. Power Electron.*, Vol. 29, No. 9, pp. 4500-4511, Sep. 2014.

[5]  J. Li, "Wireless power transmission: State-of-arts in technologies," *in Proceeding of Asia-Pacific Microwave Conference*, pp. 86-89, 2011.

[6]  T. I. Anowar, N. Kumar, H. Ramiah, and A. W. Reza, "Efficiency enhancement of wireless power transfer with

[7]  J. Dai and D. C. Ludois, "A survey of wireless power transfer and a critical comparison of inductive and capacitive coupling for small gap applications," *IEEE Trans. Power Electron.*, Vol. 30, No. 11, pp. 6017-6029, Mar. 2015.

[8]  F. Lu, H. Zhang, H. Hofmann, and C. C. Mi, "An inductive and capacitive combined wireless power transfer system with LC-compensated topology," *IEEE Trans. Power Electron.*, Vol. 31, No. 12, pp. 8471-8482, Jan. 2016.

[9]  K. H. Yi, "6.78MHz Capacitive Coupling Wireless Power Transfer System," *J. Power Electron.*, Vol. 15, No. 4, pp. 987-993, Jul. 2015.

[10]  C. K. Lee, W. X. Zhong, and S. Y. R. Hui, "Effects of magnetic coupling of nonadjacent resonators on wireless power domino-resonator systems," *IEEE Trans. Power Electron.*, Vol. 27, No. 4, pp. 1905-1916, Sep. 2012.

[11]  A. P. Sample, D. A. Meyer, and J. R. Smith, "Analysis, experimental results, and range adaptation of magnetically coupled resonators for wireless power transfer," *IEEE Trans. Ind. Electron.*, Vol. 58, No. 2, pp. 148-157, Mar. 2011.

[12]  G. A. Covic and J. T. Boys, "Inductive power transfer," *The IEEE*, Vol. 101, No. 6, pp. 1276-1289, Jun. 2013.

[13]  B. H. Lee, Y. W. Choi, and B. C. Kim, "Standby power reduction method for wireless power transfer system with parallel resonance type resonator," in *Proc. IEEE Wireless Power Transfer Conference 2016*, Aveiro, pp. 1-3, 2016.

[14]  *Wireless Power Consortium*, https://www. Wirelesspower consortium.com/

[15]  *AirFuel Alliance*, http://airfuel.org/

[16]  A. Grebennikov and A. O. Sokal, *Switchmode RF Power Amplifiers*, Newnes/Elsevier, 2007.

[17]  C. S. Wang, G. A. Covic, and O. H. Stielau, "Power transfer capability and bifurcation phenomena of loosely coupled inductive power transfer systems," *IEEE Trans. Ind. Electron.*, Vol. 51, No. 1, pp. 148-157, Feb. 2004.

[18]  S. Liu, M. Liu, M. Fu, C. Ma, and X. Zhy, "A high-efficiency class-E power amplifier with wide-range load in WPT systems," in *Proc. IEEE Wireless Power Transfer Conference 2015*, pp. 1-3, 2015.

[19]  J. J. Casanova, Z. N. Low, and J. Lin, "Design and optimization of a class-E amplifier for a loosely coupled planar wireless power system," *IEEE Trans. Circuits Syst. II*, Vol. 56, No. 11, pp. 830-834, Nov. 2009.

[20]  G. Hanington, P. F. Chen, P. M. Asbeck, and L. E. Larson, "High-efficiency power amplifier using dynamic power-supply voltage for CDMA applications," *IEEE Trans. Microw. Theory Techn.*, Vol. 47, No. 8, pp. 1471-1476, Aug. 1999.

[21]  N. O. Sokal and A. D. Sokal, "High-efficiency tuned switching power amplifier," *US Patent 3,919,656*, Nov., 1975

[22]  N. O. Sokal and A. D. Sokal, "Class E-A new class of high-efficiency tuned single-ended switching power amplifiers," *IEEE J. Solid-State Circuits*, Vol. 10, No. 3, pp. 168-176, Jun. 1975.

[23]  F. H. Raab, "Idealized operation of the class E tuned power amplifier," *IEEE Trans. Circuits Syst.*, Vol. 24, No. 12, pp.

725-735, Dec. 1977.

[24] F. H. Raab and N. O. Sokal, "Transistor power losses in the class E tuned power amplifier," *IEEE J. Solid-State Circuits*, Vol. 13, No. 6, pp. 912-914, Dec. 1978.

[25] E. C. Gomes, L. A. R. Souza, and S. Y. C. Catunda, "State space control for buck converter using decoupled block diagram approach," in *Proceeding of Brazilian Power Electronics Conference 2009*, Bonito-Mato Grosso do Sul, Brazil, pp. 686-692, 2009.

[26] P. M. Shabestari, G. B. Gharehpetian, G. H. Riahy, and S. Mortazavian, "Voltage controllers for DC-DC boost converters in discontinuous current mode," in *Proceeding of International Energy and Sustainability Conference 2015*, pp. 1-7, 2015.

[27] *Energy Star*, https://energy.gov/eere/femp/low-standby-power-product-purchasing-requirements-and-compliance-resources

[28] B. H. Lee, K. B. Park, C. E. Kim, and G. W. Moon, "No-load power reduction technique for ac/dc adapters," *IEEE Trans. Power Electron.*, Vol. 27, No. 8, pp. 3685-3694. Aug. 2012.

[29] ON Semiconductor, *NCP1237 Application Note*, https://www.onsemi.com/pub/Collateral/AND8327-D.PDF

[30] ON Semiconductor, *FAN6100Q Datasheet*, http://www.onsemi.com/pub/Collateral/FAN6100Q-D.pdf

**Byoung-Hee Lee** received his B.S., M.S. and Ph.D. degrees from the Korea Advanced Institute of Science and Technology (KAIST), Daejeon, Korea, in 2005, 2008 and 2012, respectively. From 2012 to 2015, he was a Senior Researcher at Samsung Electronics, Suwon, Korea. Since 2015, he has been working as an Assistant Professor in the Department of Electronics and Control Engineering, Hanbat National University, Daejeon, Korea. He is an Associate Editor of the Journal of Power Electronics. His current research interests include the design of power converters, wireless power transfer systems, power systems for railway cars, and battery management systems.